Technical Report No. 32-714

Experimentally Measured Effects of the Wall Boundary Layer on Shock-Tube Performance

F. R. Livingston

jpl

JET PROPULSION LABORATORY
CALIFORNIA INSTITUTE OF TECHNOLOGY
PASADENA, CALIFORNIA

March 1, 1965

Technical Report No. 32-714

Experimentally Measured Effects of the Wall Boundary Layer on Shock-Tube Performance

F. R. Livingston

Bain Dayman, Jr.

Bain Dayman, Jr., *Chief*
Aerodynamics Facilities Section

JET PROPULSION LABORATORY
CALIFORNIA INSTITUTE OF TECHNOLOGY
PASADENA, CALIFORNIA

March 1, 1965

Prepared Under Contract No. NAS 7-100
National Aeronautics & Space Administration

CONTENTS

TABLES

FIGURES

FIGURES (Cont'd)

ABSTRACT

19269

Shock speed and test time have been measured in a 3-in.-D shock tube. The shock tube is being evaluated as the hot gas supply for a 43-in.-D shock tunnel. Nitrogen was used as the test gas in the experiment, with hydrogen as the driver gas. Shock speeds compare favorably with the ideal shock-tube theory, corrected for laminar and turbulent wall-boundary-layer effects. Measured test time is shown to agree with the laminar wall-boundary-layer theory of Mirels at initial nitrogen pressures below 10 mm Hg. Test times approach the turbulent wall-boundary-layer estimate of Mirels at an initial pressure of 100 mm Hg.

AUTHOR

I. INTRODUCTION

The nitrogen driven-gas wall-boundary-layer effects and the hydrogen driver-gas thermodynamic effects on shock speed and test time were investigated experimentally in a 3-in.-D shock tube. In order to obtain the shock velocities in nitrogen of from 5300 to 13,500 ft/sec in the unheated shock tube, hydrogen was used as the driver gas. Hydrogen driver pressure was held constant at 35 atm for all tests, while the nitrogen driven-gas pressure was varied from 0.15 to 100 mm Hg. Both the ideal- and equilibrium-gas assumptions were used to compute the hydrogen driver performance. Nitrogen shock properties used in computations were those of Ahtye and Peng. Measured test time is compared to both the laminar and turbulent wall-boundary-layer theories of Mirels.

II. DESCRIPTION OF SHOCK TUBE

A. Basic Shock Tube

The 3-in.-D shock tube[1] shown in Fig. 1 has a 17-ft-long driven section and a 5-ft-long driver. The shock tube is also shown schematically in Fig. 2. Since a 5-ft driver was not required for this experiment, a 3.5-ft aluminum plug was placed in the driver to conserve the hydrogen driver gas. In order to adjust the driver pressure to the precise firing level, a double diaphragm technique was used. Square diaphragms with an opening of 2.125 in. on a side were used in this shock tube.

A mechanical pump evacuates the driver to several microns pressure prior to filling with hydrogen. An oil

[1]The 3-in. shock tube was designed by Dr. D. Collins and constructed by Mr. R. Lee of the Jet Propulsion Laboratory.

Fig. 1. Photograph of 3-in.-D shock tube

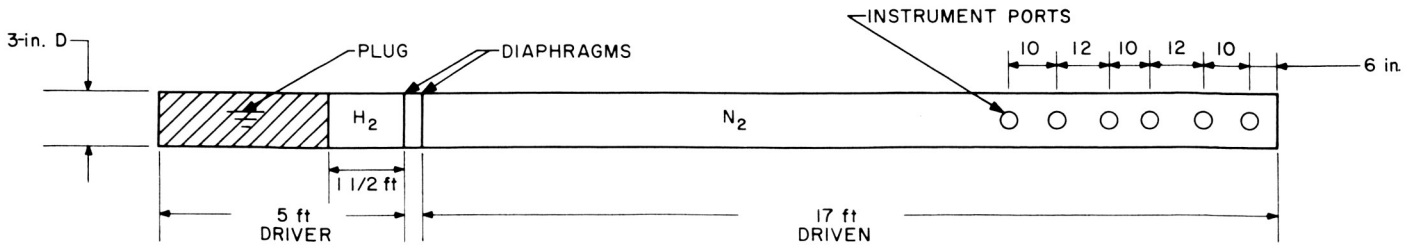

Fig. 2. Schematic diagram of 3-in.-D shock tube

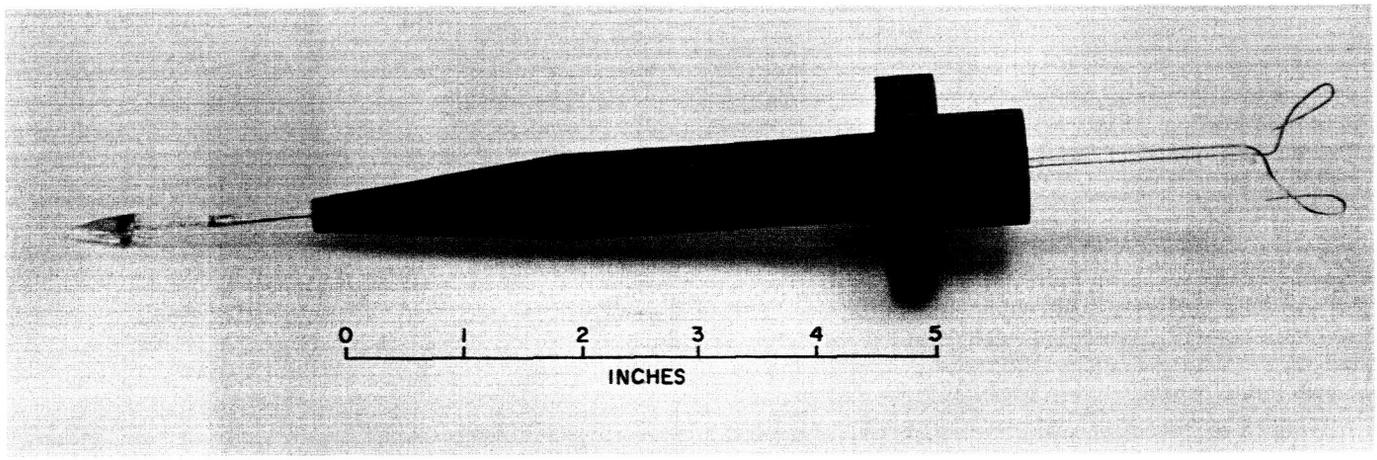

Fig. 3. Photograph of the thin-film probe

diffusion pump backed by another mechanical pump can reduce the pressure in the driven tube to 2×10^{-4} mm Hg in about 15 min.

B. Instrumentation

1. Test-Time Measurement

The duration of uniform flow behind the incident shock was measured with a thin-film probe extending 6 in. from the end plate of the shock tube. The gage design is the same as that of Holder and Schultz (Ref. 1). First, a thin-platinum film near the tip of the glass probe (Fig. 3) is heated by the passage of the shocked nitrogen (Fig. 4); then it is cooled by the hydrogen driver gas, and finally reheated by the reflected shock. Also displayed on the oscillogram is a trace of the output of the #6 thin-film detector located on the shock-tube wall at the same station as the probe. As can be seen from the oscillogram, the side-wall gage does show a slight indication of the passage of the contact surface by a discontinuity in slope.

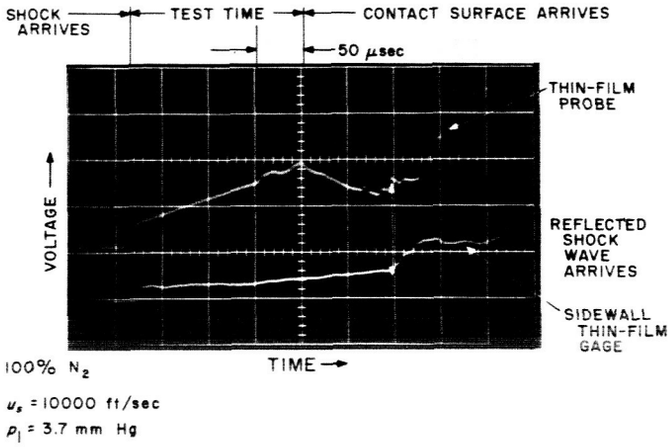

Fig. 4. Typical thin-film detector oscillogram

2. Shock-Speed Determination

Shock speed is measured by 6 thin-film thermometers spaced along the driven tube (Fig. 2). As the wall is heated by the shocked gas, the change in voltage across the thin-film detectors is amplified, mixed, and applied to the vertical axis of the raster oscilloscope, together with a sawtooth input that drives the signal vertically, as shown in the block diagram (Fig. 5). A typical raster oscillogram is shown (Fig. 6) on which the outputs of the thin-film thermometers #4, #5, and #6 are noted. The oscilloscope is triggered by a pulse from the #3 amplifier, in this case. A raster generator applies triangular pulses to the horizontal axis of the oscilloscope, and also supplies time-mark pulses to modulate the intensity of the electron beam. Sweep time can be varied by the selectron of marker, triangular, and sawtooth frequencies.

3. Nitrogen Initial-Pressure Measurement

The initial pressure of nitrogen gas in the driven tube was measured with a Wallace and Tiernan mercury manometer and/or a Wallace and Tiernan gage at pressures above 0.15 mm Hg. An oil micromanometer designed by Kendall (Ref. 2) was used to calibrate the other gauges at pressures between 12 and 0.0 mm Hg with an accuracy of ± 5-μ Hg.

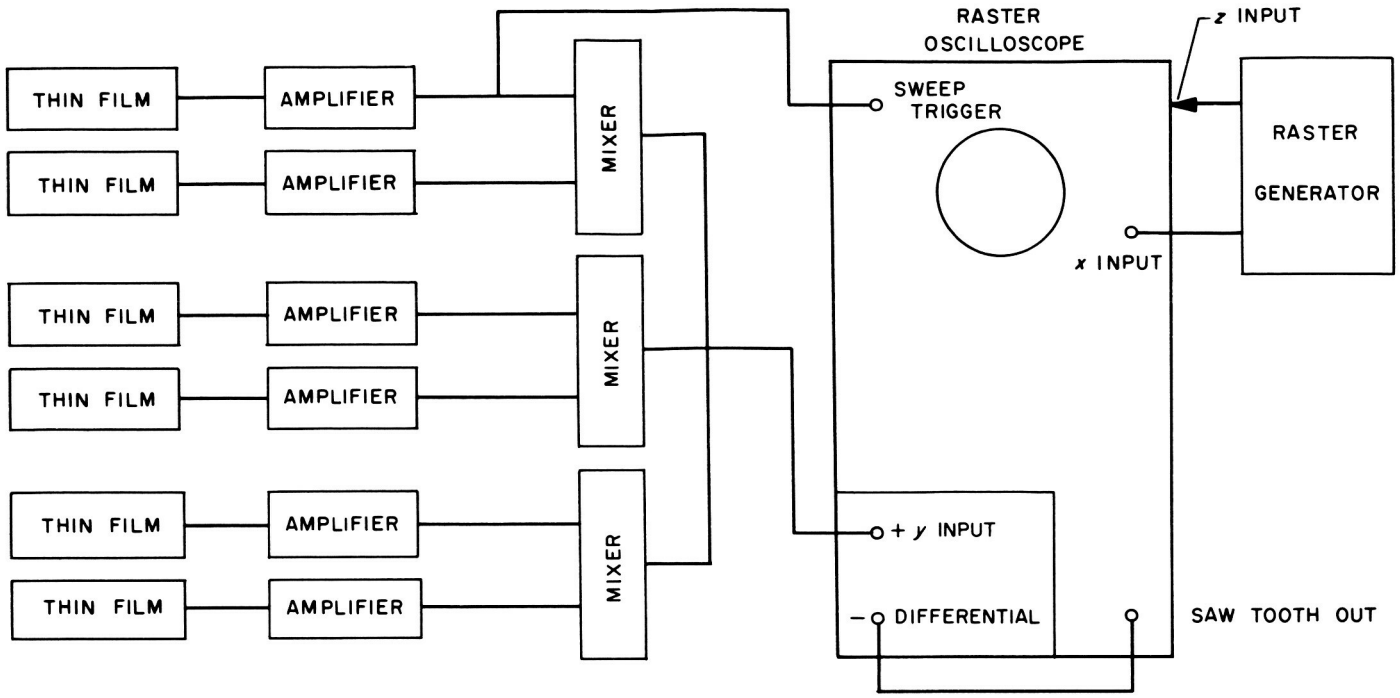

Fig. 5. Block diagram of the shock-speed measuring system

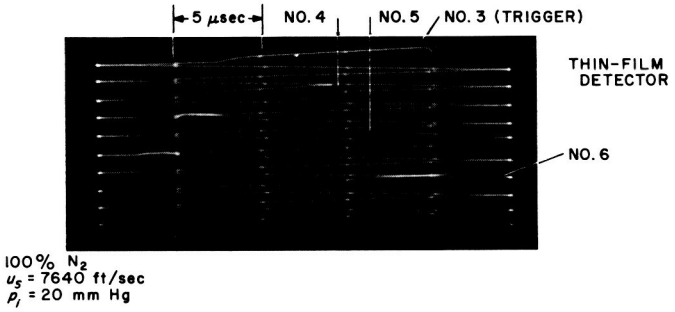

Fig. 6. Typical raster oscillogram

III. SHOCK-SPEED CALCULATIONS AND MEASUREMENTS

A. Ideal H_2 Driver Gas/Equilibrium, Viscous N_2 Driven Gas

1. Ideal Shock-Tube Performance

For the calculations presented in this Section, the hydrogen driver gas is treated as an ideal gas with an isentropic expansion coefficient γ equal to 7/5, and with a sound speed a_4 of 4260 ft/sec at room temperature. The nitrogen driven gas is treated as an equilibrium real gas in all cases, since the vibration relaxation time has been measured to be 25 μsec by Blackman (Ref. 3) at these test conditions. Equilibrium nitrogen dissociation will be generally less than 5% at these test conditions. At the initiation of flow in this 3-in.-D shock tube, a centered expansion wave moves into the driver from the 2.125-in. square diaphragm opening. Steady flow exists at the diaphragm station with sonic speed at the orifice, while a compression process or expansion wave is carried into the driven tube (Fig. 7).

All driver-gas flow parameters were arrived at by methods described by Russell (Ref. 4) for a shock tube with area change near the diaphragm. The steady compressible flow functions tabulated by the Ames Research Staff (Ref. 5) and by Wang, Peterson and Anderson (Ref. 6), and flow functions for a simple nonsteady expansion wave tabulated by Roshko and Rubenstein (Ref. 7) are convenient to use for the calculations. By use of these tables, it is a straightforward task to obtain

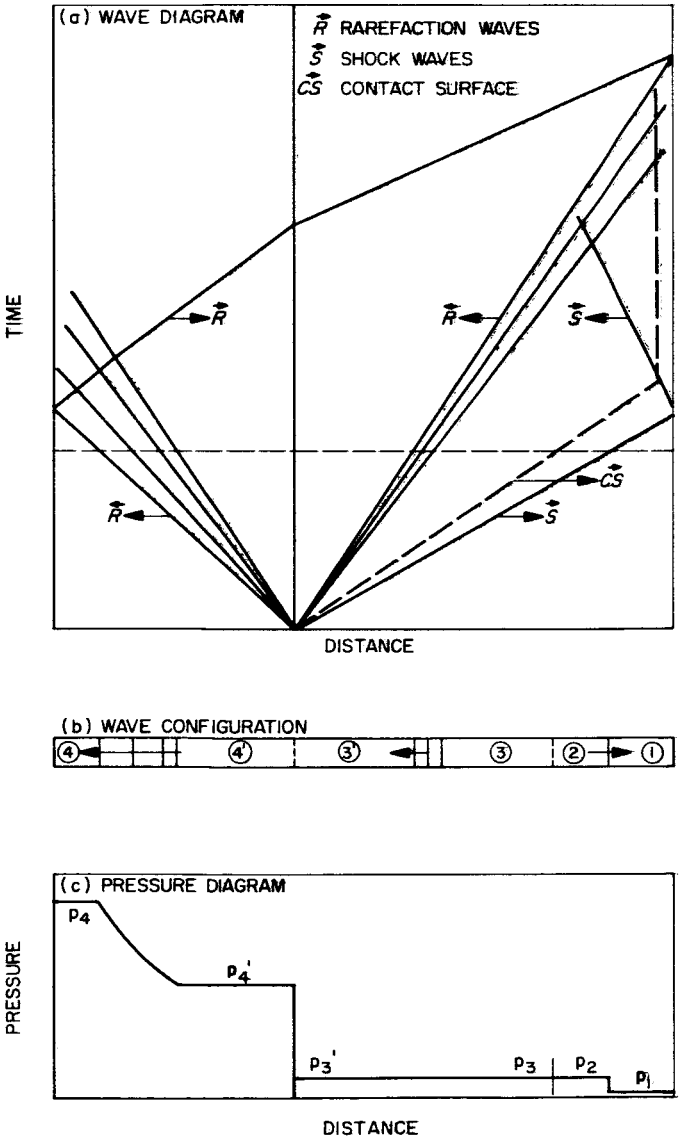

Fig. 7. Wave and pressure diagrams and wave configuration of 3-in. shock tube

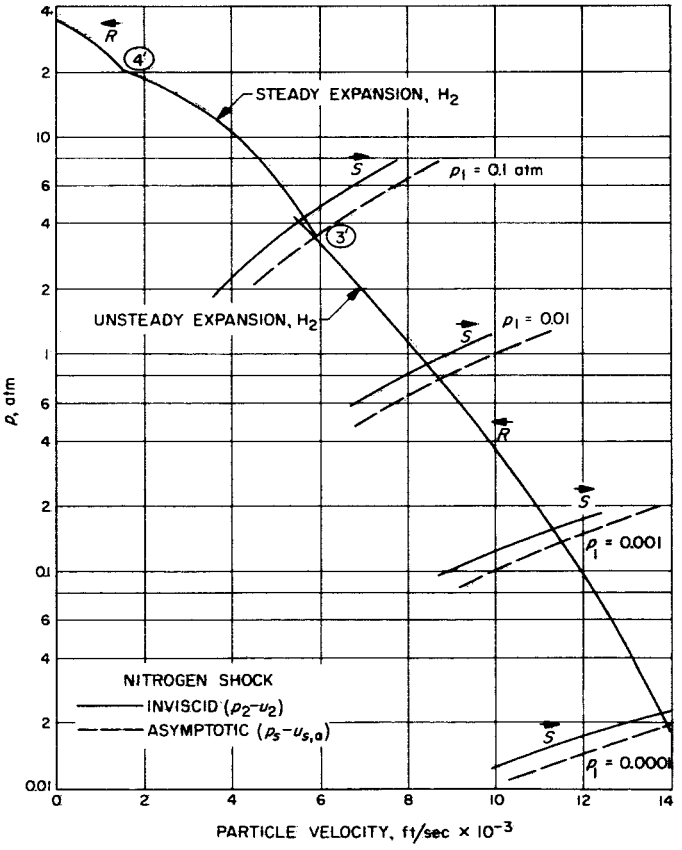

Fig. 8. Pressure-velocity diagram: ideal H_2 driver gas; equilibrium N_2 driven gas

all flow properties in ideal expanding flows for driver-gas isentropic exponents of 7/5 or 5/3.

Computed values of contact surface pressure p_3 are plotted as a function of particle velocity u_3 (Fig. 8). With the p–u diagram, it is possible to solve the shock-tube equations graphically if, in addition to driver performance, the nitrogen shock properties are known. The thermodynamic properties of high-temperature nitrogen behind an incident shock wave, obtained from Ahtye and Peng (Ref. 8), are tabulated in Table 1 for the pressure-velocity range of interest in this experiment. The pressure p_2 behind the incident shock is illustrated in Fig. 8. A solution to particle velocity u_2 occurs where the shock p_2–u_2 curve intersects the driver p_3–u_3 curve. Initial nitrogen pressure p_1 is shown as 0.1, 0.01, 0.001, and 0.0001 atm. Driver pressure p_4 is 35 atm. Inviscid shock speed $u_{s,i}$ is computed from the particle speed u_2 as follows:

$$u_{s,i} = \frac{u_2}{1 - \rho_1/\rho_2}$$

where ρ_1/ρ_2 = density ratio across the shock.

The theoretically ideal driver-gas solution is plotted in Fig. 9 showing the variation of shock speed with initial nitrogen pressure. Particle velocity and the asymptotic

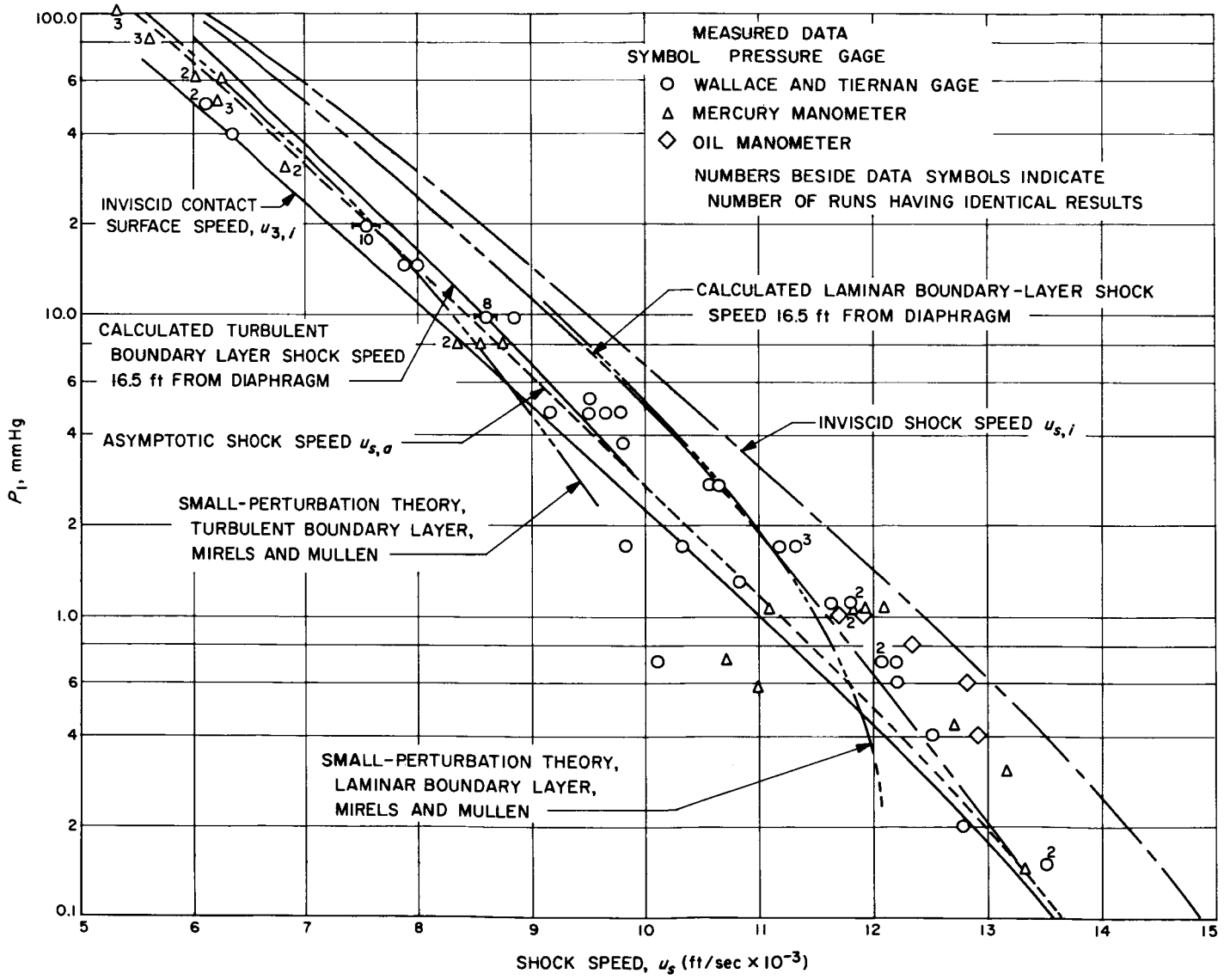

Fig. 9. Shock-speed variation with initial pressure: ideal H_2 driver gas; equilibrium N_2 driven gas

Table 1. Nitrogen normal-shock properties

$a_1 = 1143$ ft/sec $\qquad T_1 = 293°K$

M_s	u_1, ft/sec	Initial Nitrogen Pressure, p_1															
		0.1 atm				0.01 atm				0.001 atm				0.0001 atm			
		p_2/p_1	ρ_2/ρ_1	T_2/T_1	u_2, ft/sec	p_2/p_1	ρ_2/ρ_1	T_2/T_1	u_2, ft/sec	p_2/p_1	ρ_2/ρ_1	T_2/T_1	u_2, ft/sec	p_2/p_1	ρ_2/ρ_1	T_2/T_1	u_2, ft/sec
4	4536	18.759	4.84	3.885	3630												
5	5715	29.655	5.5	5.382	4675												
6	6858	43.001	6.01	7.163	5720	43.001	6.01	7.163	5720	43.001	6.01	7.163	5720				
7	8001	58.824	6.424	9.203	6753	58.824	6.424	9.203	6753	58.824	6.424	9.203	6753				
8	9144	77.256	6.678	11.582	7772	77.256	6.678	11.582	7772	77.256	6.678	11.582	7772	77.256	6.69	11.515	7772
9	10287					98.009	7.007	14.053	8816	98.386	7.007	13.819	8816	98.6	7.35	13.419	8816
10	11430					122.092	7.428	16.332	9887	123.024	7.714	15.639	9944	123.8	8.170	14.824	9943
11	12573									150.588	8.643	16.786	11114	151.7	9.225	15.563	11114
12	13716									181.392	9.626	17.711	12289	182.1	10.38	16.409	12289
13	14880									....	10.5	18.522	13420				
14	16000									....	11.4	19.213	14600				

shock speed $u_{s,a}$ are also shown as a function of initial pressure.

2. Viscous Correction to Shock-Tube Performance

For the asymptotic condition of viscous flow in the shock tube, Duff (Ref. 9) has found the driver-gas velocity u_3 to equal the asymptotic shock velocity $u_{s,a}$. As suggested by Mirels (Ref. 10), the stagnation pressure behind the shock, relative to the contact surface, is computed and plotted (Fig. 8) in order to solve for the asymptotic shock speed. The incompressible equation used to compute stagnation pressure in the subsonic flow of shocked gas, with respect to the contact surface, is

$$p_s = p_2 + \frac{1}{2}\rho_2 (u_1 - u_2)^2$$

The solution for the asymptotic shock speed occurs where the stagnation-pressure curve intersects with the driver expansion-wave curve in Fig. 8.

To compute the shock speed corrected for viscous effects at a point 16.5 ft from the diaphragm, it was necessary (1) to assume either laminar or turbulent flow, and (2) to estimate the viscous shock speed for a given initial driven-gas pressure, p_1. The computation required knowledge of the maximum test-slug length l_m, the nondimensional distance from the diaphragm X, and the nondimensional contact-surface-to-shock separation distance T all defined and derived by Mirels (Refs. 10 and 11) and Roshko (Ref. 12):

$$X = \frac{1}{W}\frac{x}{l_m}$$

$$T = l/l_m$$

where

x = distance from diaphragm

$W = \rho_2/\rho_1$ = density ratio across the shock

l = separation distance

With the theoretical values of X and T from the work of Mirels, the speed differential between the shock and contact surface is computed from

$$u_s - u_3 = \frac{dl}{dx} = \frac{dT}{dX}\frac{u_s}{W}$$

where

$$\frac{dT}{dX} = 1 - T^{1-n} \begin{cases} n = \frac{1}{2} \text{ for laminar flow} \\ n = \frac{1}{5} \text{ for turbulent flow} \end{cases}$$

The viscous shock speed at the test station was then computed by assuming that the shock speed recedes to the asymptotic shock speed in the same proportion as the contact-surface speed increases to the asymptotic value

$$u_s = \frac{(u_{s,i} - u_{s,a})}{(u_{s,i} - u_{3,i})}\left(\frac{dl}{dt}\right) + u_{s,a}$$

where

u_s = corrected shock speed

$u_{s,i}$ = inviscid shock speed

$u_{s,a}$ = asymptotic shock speed

$u_{3,i}$ = inviscid contact-surface speed

Solutions for both the turbulent and laminar wall boundary layers were made for a station 16.5 ft from the diaphragm. These solutions are plotted (Fig. 9) where correlation with measured shock speed for the near-turbulent cases $p_1 > 5$ mm Hg is remarkably good. The measured shock speed below $p_1 = 5$ mm Hg shows some scatter; however, the agreement with the laminar theory is good. Measured shock speeds at the lower pressures are about 200 ft/sec faster than the computed shock speeds. This indicates the ability to calculate the viscous shock speeds to accuracies of less than 2%, using the ideal driver-gas assumption and the wall-boundary-layer theories of Roshko and Mirels.

Also indicated in Fig. 9 are the small-perturbation-theory results of Mirels and Mullen (Ref. 13) for the condition of ideal hydrogen driving real air. The theory predicts the attenuation of the nitrogen shock quite adequately at shock speeds faster than the asymptotic shock speed to which the theory applies.

B. *Equilibrium H_2 Driver Gas/Equilibrium, Viscous N_2 Driven Gas*

Hydrogen gas at moderate pressures and 293°K temperature has a value of $\gamma = 1.40$; however, at low pressures, and at a temperature of 50°K, the isentropic

exponent equals 1.66. Rotation of the molecule under equilibrium conditions is de-excited at low temperatures, and hydrogen acts like a monatomic gas. It can be appreciated that the equilibrium expansion of hydrogen will differ somewhat from that of a perfect gas; therefore, driver performance has been computed for the equilibrium case. Glass (Ref. 14) and Trimpi (Ref. 15) have described a stepwise method to cope with this imperfect-gas effect. Any variable-entropy region is neglected, and numerical integration is performed along an isentrope. For the centered rarefaction wave, the following condition must be satisfied:

$$du = -\left(\frac{dh}{a}\right)_s$$

where

u = particle velocity

a = speed of sound

h = enthalpy of gas

s = entropy of gas

Using the hydrogen tables of Hilsenrath, et al. (Ref. 16), and Woolley, Scott and Brickwedde (Ref. 17), a step-by-step summation was made at constant entropy for the unsteady-expansion process in the driver and driven tube.

For the steady expansion through the diaphragm station, conservation of mass, momentum, and energy at constant entropy was applied in order to find all flow properties. First, to find the velocity of the gas at a lower pressure and temperature than the initial condition, the energy relationship was used

$$du = -\left(\frac{dh}{u}\right)_s$$

The continuity equation was applied to find the area ratio corresponding to a given thermodynamic state by utilizing the gas velocity as computed above and the density shown in the tables

$$\frac{A}{A^*} = \frac{\rho^* u^*}{\rho u}$$

where

A = area of channel

A^* = area at diaphragm station

The values of ρ^* and u^* were found by plotting the variation of ρ and u with Mach number. Mach number at the throat was taken as equal to 1.0, although this may not be strictly true. With this information, it was possible to obtain the entrance and exit velocity, the pressure, and the density and speed of sound at the diaphragm station.

Results of these calculations are illustrated in the p–u diagram (Fig. 10) for a driver pressure of 35 atm. Also, plotted on the same curve are the nitrogen-incident shock curves described in the foregoing Section. The calculated shock speed, contact-surface speed, and asymptotic shock speed are shown in Fig. 11. Results differ somewhat from the ideal-gas solution. At 1 mm Hg, nitrogen initial pressure in the shock tube, the ideal-gas solution, would

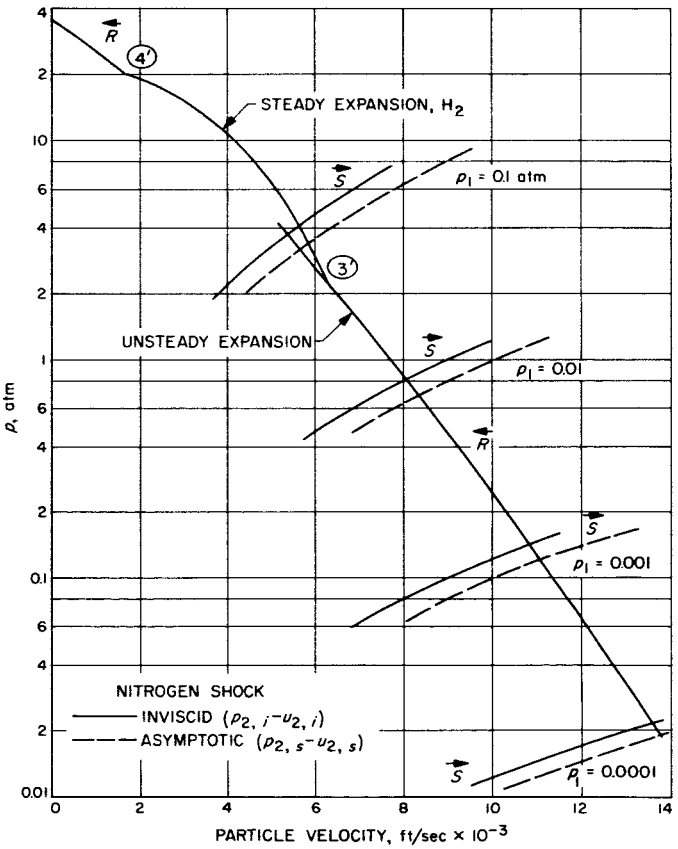

Fig. 10. Pressure-velocity diagram: equilibrium H_2 driver gas; equilibrium N_2 driven gas

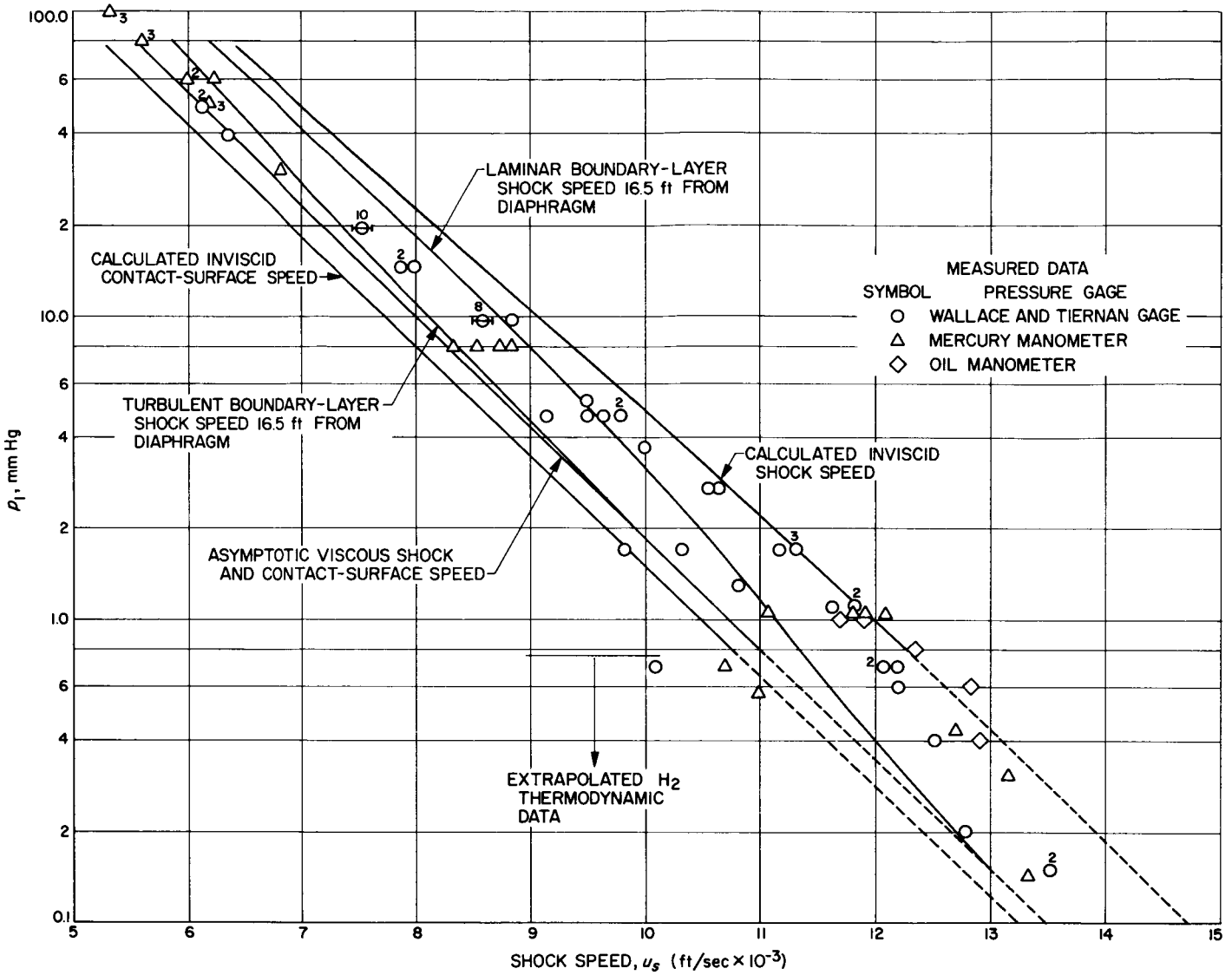

Fig. 11. Shock-speed variation with initial pressure: equilibrium H_2 driver gas; equilibrium N_2 driven gas

indicate an inviscid shock speed of 12,470 ft/sec, where the equilibrium real-gas solution for inviscid shock speed is 12,150 ft/sec. The calculated results agree with measured data at shock speeds less than 8000 ft/sec where the wall-boundary-layer flow is turbulent. Where the boundary layer is laminar, the ideal-gas solution corrected for viscous effects indicates better agreement with the measured results than the equilibrium real-gas solution.

IV. TEST-TIME CALCULATIONS AND MEASUREMENTS

Test times were calculated for both the laminar and turbulent wall boundary layer after the methods of Mirels (Refs. 10 and 11). The test station in the 3-in. D shock tube was 16.5 ft from the diaphragm. Test times computed for the 16.5-ft station are shown in Fig. 12 as a function of nitrogen initial pressure and in Fig. 13 as a function of shock speed. Runs are tabulated in Table 2. It appears as if the test time is predicted very well by the laminar boundary-layer theory up to an initial pressure of near 5 mm Hg for this experiment. At pressures between 5 and 50 mm Hg, the test-time data scatters between the laminar and turbulent theory of Mirels. Apparently the data tend to agree with the turbulent boundary-layer theory above a nitrogen initial pressure of 50 mm Hg, but additional tests would be required to verify this conclusion.

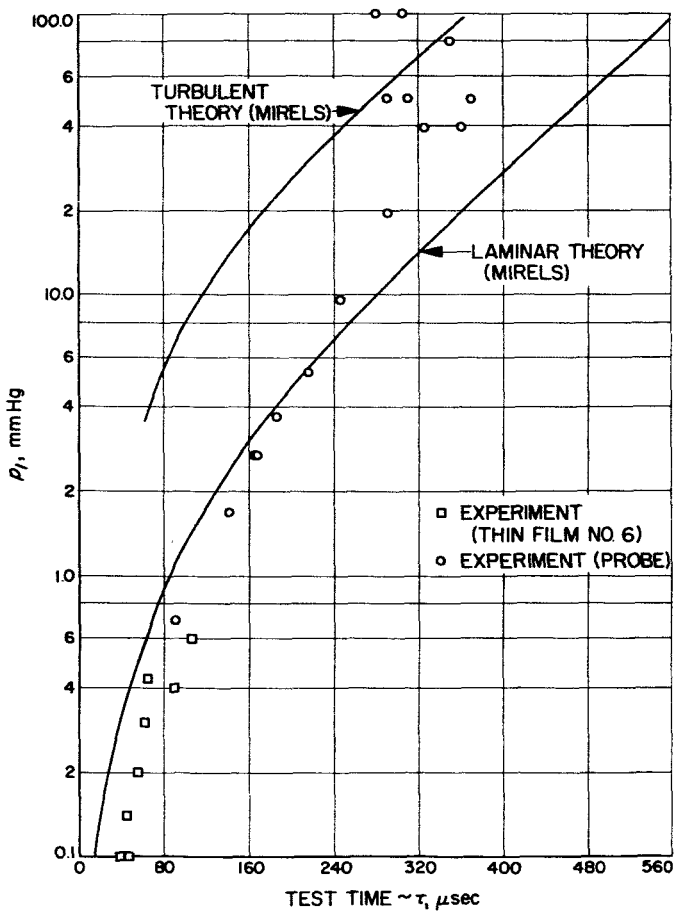

Fig. 12. Variation of test time with initial pressure

In solving for the theoretical test time, the real-air solution was thought to be applicable to these nitrogen calculations. The nondimensional shock-contact surface separation distance as calculated from the theory of Mirels (Fig. 14) is shown for both the turbulent and

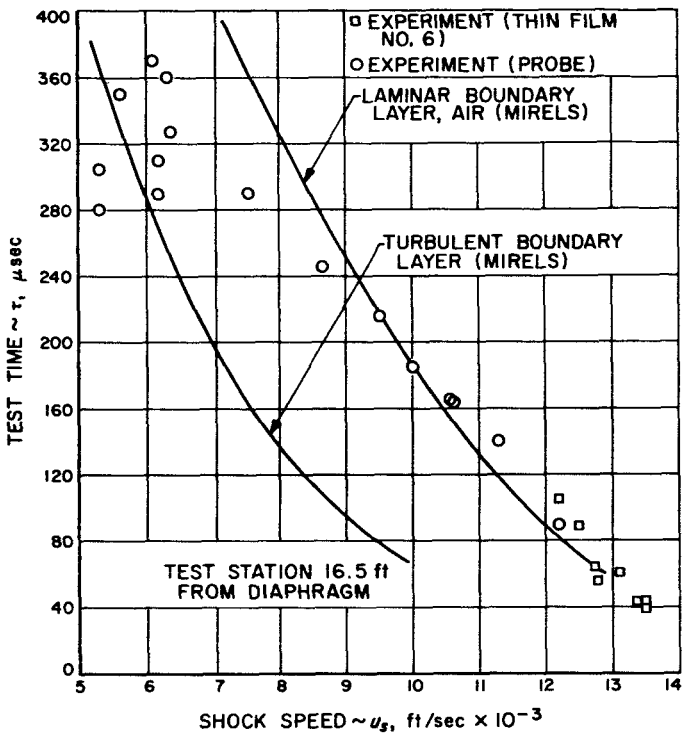

Fig. 13. Variation of test time with shock speed

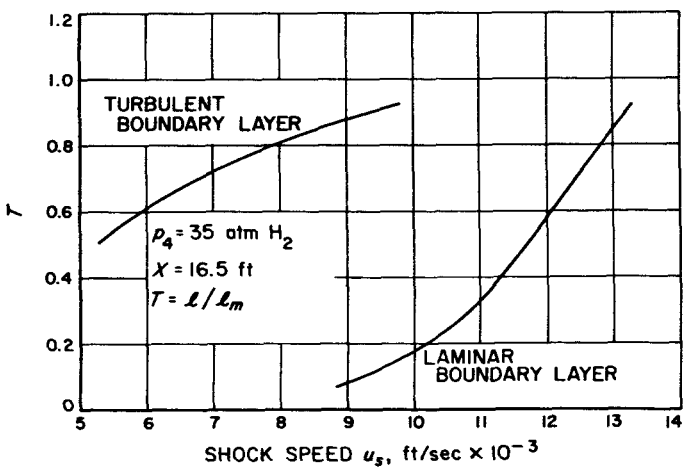

Fig. 14. Variation of the calculated nondimensional separation distance with shock speed

laminar boundary-layer cases. This is the ratio of the separation distance attained to the maximum value possible. For test conditions near 6000 ft/sec with a near-turbulent boundary layer, possibly a longer test slug can be attained by lengthening the tube. In the laminar-flow regime, test times can be increased at shock speeds above 8000 ft/sec by lengthening the tube, until at shock speeds above 13,000 ft/sec only an increase in the diameter of the shock tube or initial pressure will improve the test-time performance.

Table 2. Tabulation of runs

Hydrogen driving nitrogen

P_4 = 500 psig = 35 atm

Date	Run No.	P_1, mm Hg	u_s, ft/sec	τ, μsec
6-19-64	225	9.7	8650	245
	226	5.35	9500	215
	227	1.7	11280	140
	228	0.7	12200	90
6-22-64	231	19.7	7550	290
	232	39.7	6340	360
6-23-64	233	39.7	6390	325
	234	49.7	6120	370
	235	2.7	10560	165
	236	3.7	10000	185
	237	2.7	10640	163
6-24-64	240	80	5620	350
6-25-64	243	50	6200	290
	244	50	6210	310
	245	100	5320	280
	246	100	5350	305

Note: Table includes only runs where test time was obtained.

V. TRANSITION

Judging from Figs. 12 and 13, transition occurred near an initial pressure of 5 mm Hg at the shock speed of 9500 ft/sec (corresponding to a Mach number of 8.3 and a Reynolds number of about 6.6×10^6). The transition Reynolds number is defined (Ref. 10) as $Re_t = u_2 (W - 1)^2 l_t/\nu_2$ where u_2 = particle velocity behind the shock, l_t = distance between the shock and the transition point, and ν_2 = kinematic viscosity behind the shock. For $1 \leq M_s \leq 9$, Re_t has been observed by other experimenters to be in the range $0.5 \leq Re_t \times 10^{-6} \leq 4$.

VI. CONCLUSIONS

The Jet Propulsion Laboratory has a 3-in.-D shock tube with which it is possible to make precise measurements of shock speed and test time. Hydrogen driver gas was used to drive shocks into nitrogen at speeds from 5300 to 13,500 ft/sec.

The expected shock speeds were computed assuming both ideal and equilibrium hydrogen driver gas. The shock speeds computed from ideal shock-tube theory were corrected for viscous effects. Measured shock speeds showed good agreement with the turbulent boundary layer, equilibrium H_2 driver-gas solutions at shock speeds below 8000 ft/sec. The ideal H_2 driver gas, viscous boundary-layer solutions provide a good estimate of shock speed with an error of about ± 200 ft/sec at initial pressures less than 5 mm Hg. There is a transition of measured shock speed from the turbulent boundary-layer solution to the laminar solution near a nitrogen initial pressure of 5 mm Hg, and a shock speed of 9600 ft/sec.

At nitrogen initial pressures less than 5 mm Hg, measured test times agree with the real-air laminar wall-boundary-layer theory of Mirels. At initial pressures near 100 mm Hg, the measured test time approaches that calculated for the turbulent wall boundary layer.

NOMENCLATURE

A	area of channel
a	speed of sound
$\overrightarrow{CS}$	contact surface
D	diameter
d	differential
H_2	hydrogen molecule
h	enthalpy
l	test-slug length
M	Mach number
N_2	nitrogen molecule
n	boundary-layer exponent
p	absolute pressure

NOMENCLATURE (Cont'd)

$\vec{R}$ rarefaction wave

Re Reynolds number

$\vec{S}$ shock wave

s entropy

T nondimensional contact surface to shock separation distance

T temperature

u particle velocity in laboratory coordinates

W density ratio, ρ_2/ρ_1

X nondimensional distance from diaphragm

x distance from diaphragm

γ isentropic expansion coefficient

μ absolute viscosity

ν kinematic viscosity, $\frac{\mu}{\rho}$

ρ density

τ test time

Subscripts

$_1$ initial condition in driven tube

$_2$ condition behind the shock

$_3$ condition behind the contact surface

$_4$ initial condition in driver tube

$_a$ asymptotic flow condition

$_i$ inviscid flow condition

$_m$ maximum

$_s$ shock condition

$_t$ transition

Superscripts

* conditions at diaphragm station

$'$ conditions after flow has started

REFERENCES

1. Holder, D. W., and D. L. Schultz, "On the Flow in a Reflected-Shock Tunnel", Aeronautical Research Council, *A.R.C. 22, 152*, August 29, 1960.
2. Kendall, J. M., "The Design and Performance of Precision Oil Micromanometers", *NAVORD Report 6803*, U. S. Naval Ordnance Laboratory, White Oak, Maryland, June 29, 1961.
3. Blackman, V., "Vibration Relaxation in Oxygen and Nitrogen", *Jour. of Fluid Mech.*, Vol. 1, 1956.
4. Russell, D. A., "A Study of Area Change Near the Diaphragm of a Shock Tube", Guggenheim Aeronautical Laboratory, California Institute of Technology, *Memorandum No. 57*, July 20, 1960.
5. Ames Research Staff, "Equations, Tables and Charts for Compressible Flow", *NACA Report 1135*, 1953.
6. Wang, C. S., J. B. Peterson, and R. Anderson, "Gas Flow Tables", Space Technology Laboratories, Inc., *GM-T12-154*, March 14, 1957.
7. Roshko, A., and M. Rubenstein, "Tables of Flow Functions for a Simple Nonsteady Expansion Wave", Douglas Aircraft Company, Inc., *ES 40031*, September 1, 1960.
8. Ahtye, W. F., and Tzy-Cheng Peng, "Approximation for the Thermodynamic and Transport Properties of High-Temperature Nitrogen with Shock-Tube Applications", *NASA TN D-1303*, Washington, July, 1962.
9. Duff, R., "Shock-Tube Performance at Low Initial Pressure", *The Physics of Fluids*, Vol. 2, No. 2, March–April, 1959.
10. Mirels, H., "Test Time in Low Pressure Shock Tubes", *The Physics of Fluids*, Vol. 6, No. 9, September, 1963.
11. Mirels, H., "Shock Tube Test Time Limitation Due to Turbulent-Wall Boundary Layer", *AIAA Journal*, Vol. 2, No. 1, January, 1964.
12. Roshko, A., "On Flow Duration in Low Pressure Shock Tubes", *The Physics of Fluids*, Vol. 3, No. 6, November–December, 1960.
13. Mirels, H., and J. F. Mullen, "Small Perturbation Theory for Shock Tube Attenuation and Nonuniformity", *The Physics of Fluids*, Vol. 7, No. 8, August, 1964.
14. Glass, I. I., "Shock Tubes, Part I: Theory and Performance of Simple Shock Tubes", Institute of Aerophysics, University of Toronto, May, 1958.
15. Trimpi, R. L., "A Preliminary Study of a New Device for Producing High-Enthalpy, Short Duration Gas Flows", *Advances in Hypervelocity Techniques*, Plenum Press, New York, 1962.
16. Hilsenrath, J., et al., "Tables of Thermal Properties of Gases", *NBS Circular 564*, November 1, 1955.
17. Woolley, H. W., R. B. Scott, and F. G. Brickwedde, "Completion of Thermal Properties of Hydrogen in Its Various Isotopic and Ortho-Para Modifications", U. S. Bureau of Standards, *J. Research*, Vol. 41, No. 5, November, 1948.

ACKNOWLEDGMENT

The author would like to acknowledge the work of Mr. Michael McKenna, who conducted many of the shock-tube tests, reduced the data, and performed analytical computations. Mr. David Etheridge of the Hypervelocity Laboratory constructed the thin-film thermometers used in these tests, and was helpful in the operation of the test equipment.